Active cell movements coupled to positional induction are involved in lineage segregation in the mouse blastocyst

Sigolène M. Meilhac[1,4], **Richard J. Adams**[2,+], **Samantha A. Morris**[1,+], **Anne Danckaert**[3], **Jean-François Le Garrec**[4], and **Magdalena Zernicka-Goetz**[1,*]

[1]Gurdon Institute, University of Cambridge, Tennis Court Road, Cambridge, CB2 1QN, UK

[2]Department of Physiology, Development and Neuroscience, University of Cambridge, Cambridge, CB2 3DY, UK

[3]Institut Pasteur, PFID, Paris, France

[4]Institut Pasteur, Department of Developmental Biology, CNRS URA2578, Paris, 75015, France

Abstract

In the mouse blastocyst, some cells of the inner cell mass (ICM) develop into primitive endoderm (PE) at the surface, while deeper cells form the epiblast. It remained unclear whether the position of cells determines their fate, such that gene expression is adjusted to cell position, or if cells are pre-specified at random positions and then sort. We have tracked and characterised dynamics of all ICM cells from the early to late blastocyst stage. Time-lapse microscopy in H2B-EGFP embryos shows that a large proportion of ICM cells change position between the surface and deeper compartments. Most of this cell movement depends on actin and is associated with cell protrusions. We also find that while most cells are precursors for only one lineage, some give rise to both, indicating that lineage segregation is not complete in the early ICM. Finally, changing the expression levels of the PE marker Gata6 reveals that it is required in surface cells but not sufficient for the re-positioning of deeper cells. We provide evidence that Wnt9A, known to be expressed in the surface ICM, facilitates re-positioning of Gata6-expressing cells. Combining these experimental results with computer modelling suggests that PE formation involves both cell sorting movements and position-dependent induction.

Keywords

mouse blastocyst; cell lineage; cell movement; Gata6; Wnt; inner cell mass; primitive endoderm

Introduction

During blastocyst development a group of ICM cells are set aside and retain pluripotency to give rise to the epiblast, the future foetus, while other cells differentiate into the primitive endoderm (PE), an extra-embryonic tissue that will contribute to the yolk sac. PE differentiation becomes visible by 4.5 days after fertilisation (E4.5) when PE cells adopt a distinct morphology (Nadijcka and Hillman, 1974) and express transcription factors, such as Gata4 and Gata6, required for their differentiation (Kuo et al., 1997; Molkentin et al., 1997; Morrisey et al., 1998; Koutsourakis et al., 1999). At this stage, PE cells have a restricted lineage potential (Gardner and Rossant, 1979). However, the extent to which ICM cells are

[*]corresponding author: m.zernicka-goetz@gurdon.cam.ac.uk phone 0044 1223 763 291 fax 0044 1223 334 089 .
[+]These authors contributed equally to this work

initially bipotent, meaning contribute to both lineages, at E3.5 remains unknown (Gardner, 1983 ; Weber et al., 1999; Chazaud et al., 2006; Perea-Gomez et al., 2007). Consequently, it remains unclear when and how segregation between PE and epiblast lineages is accomplished.

Two sets of observations led to two alternative models for this cell fate decision. First is the position-based model which stems from the fact that PE cells lie at the surface of the ICM, so that cell position would be the factor determining their specification (Rossant, 1975; Gardner, 1983). This is supported by the observations that only cells on the periphery of embryonal carcinoma aggregates respond to endoderm-inducing cues (Murray and Edgar, 2004). Alternatively, a model of sorting of earlier pre-specified cells was suggested. This is based on the expression of epiblast and PE markers such as Nanog and Gata6. Before the PE differentiates, the cells expressing these genes are intermingled and localised in both deeper and surface compartments of the early ICM (Chazaud et al., 2006; Plusa et al., 2008). Gene profiling of ICM or ES cells also revealed the heterogeneity of the ICM cell population (Kurimoto et al., 2006 ; Singh et al., 2007). These results suggest two possible mechanisms for PE formation. Cells with specific molecular identity (i.e. expressing either PE or epiblast markers) sort out to reach a position corresponding to their destiny, thus implying cell movement. Alternatively, initial gene expression patterns become "adjusted" such that PE marker genes become down-regulated in deeper cells and up-regulated in surface cells and vice versa for markers of the epiblast. Indeed, *Nanog* expression fluctuates in ES cells (Chambers et al., 2007). Time-lapse experiments in a transgenic line following a specific subgroup of cells expressing the PE marker PDGFRα have shown that these cells both move and have fluctuating expression levels of this marker (Plusa et al., 2008). However it remains unclear whether all ICM cells move, what is the mechanism of this movement and whether the elevated expression of some transcription factors key for these cell fate decisions is enough for cell sorting.

To address these questions we have characterised the behaviour, nature of movement and lineage segregation of all cells within the ICM. This and computer modelling indicate that both position-dependent induction and cell sorting movements participate in PE and epiblast lineage segregation.

Materials and methods

Embryo culture

Embryos were collected from matings of spontaneously ovulating females F1 (C57BL/6xCBA) with transgenic *H2B-EGFP* mice (Hadjantonakis and Papaioannou, 2004). Early blastocysts, which had not completed their sixth cleavage division, were flushed from the uterus in M2 medium and cultured as before (Bischoff et al, 2008). To test the effect of drugs, KSOM was supplemented with 1.6 ng/mL of nocodazole (Sigma) or 1 µg/mL of cytochalasin D (Sigma). All experiments with animals were conducted in accordance with UK Government Home Office Licensing regulations.

Time-lapse imaging

Embryos were cultured and imaged in 4D in a glass-bottom dish (MatTek) on an inverted epifluorescent Zeiss Axiovert 200M microscope with a 20X/0.75NA objective. Multi-channel (red-fluorescence/green-fluorescence/transmission) multi-section images were acquired every 10 or 15 minutes as before (Bischoff et al., 2008). In two-channel (green/transmission) movies, 12 focal planes were acquired every 5 µm, with an exposure of 4 ms for transmitted light and 400 ms for green fluorescence, using a 30% cut neutral density filter from Chroma. In three-channel movies, 9 focal planes were acquired every 6-7 µm,

with an exposure of 4 ms for transmitted light, 70 ms for green fluorescence and 50 ms for red fluorescence, using a 50% cut neutral density filter from Chroma.

Phalloidin staining and immunostaining

Phalloidin staining was performed as previously (Perea-Gomez et al., 2007) and immunostaining as described (Torres-Padilla and Zernicka-Goetz, 2006 ; Plusa et al., 2008) with anti-Gata4 (Santa Cruz C20) anti-Gata6 (Santa Cruz H92), anti-Nr2f1 (Abcam 3830) and β-catenin (Sigma C3306) antibodies and counterstained with Hoechst or TOTO-3. Images were acquired on a Leica TCS SP5 confocal microscope with a 40X oil objective or on a BioRad Radiance 2100 confocal microscope with a 20X objectiv. β-catenin staining intensities were measured in Image J.

Plasmids used and cloned

Red fluorescent RFP and GAP-RFP templates were derived from *mRFP1* (Campbell et al., 2002) and cloned into a pBluescriptRN3P vector (Lemaire et al., 1995) containing globin 5′ and 3′ UTRs. Oligonucleotides GAP-F 5′- GATCCATGCTGTGCTGTATGAGAAGAACCAAACAGGTTGAAAAGAATGATGAG GACC AAAAGATTGGA and GAP-R 5′- GATCTCCAATCTTTTGGTCCTCATCATTCTTTTCAACCTGTTTGGTTCTTCTCATA CAGC ACAGCATG were used to add a GAP43 membrane localisation signal (Moriyoshi et al., 1996).

Full-length mouse cDNA of Gata6 (Liang et al., 2001) and Wnt9A (IMGCLO30435371 clone from Geneservice Ltd) were cloned into the RN3P vector for over-expression experiments. The same vector was used for Gata6 dominant-negative (GDN template, Yang et al., 2002), *Nr2f1* dominant-negative (CDN template, Adam et al., 2000). WDN template encodes a defective Wnt9A ligand, deleted for the C-terminal cysteine-rich domain (see Fig. 4A), analogous to previously generated dominant-negative Wnts (Hoppler et al., 1996; Tada and Smith, 2000). A similar Wnt9A[DN] construct was shown to function as a dominant-negative (Person et al., 2005). It was amplified by PCR using the oligonucleotides WDN-F 5′- GAAGATCTACAAGAGGTAATCCAGCG and WDN-R 5′- CGGAATTCGCAGAAGCTGGGAGAGTC. All the constructs were verified by sequencing.

Microinjection of blastocyst cells

For preparation of synthetic capped mRNA, the plasmids were linearised, and transcribed in vitro using the mMESSAGEmMACHINE kit (Ambion). Capped mRNA was purified from proteins with phenol/chloroform and from nucleotides on an Rneasy MinElute Cleanup column (Qiagen). For microinjection, mRNA was diluted at a final concentration of 0.07-0.25 μg/μl.

Microinjection of RNA was performed as previously described (Zernicka-Goetz et al., 1997; Weber et al., 1999; Perea-Gomez et al., 2007). Deeper and surface ICM cells were injected through the polar and mural trophectoderm respectively. Positive embryos were screened about 1 h after injection, when the embryos had recovered and the fluorescent protein was expressed. RFP- injections did not significantly change the proliferation or survival of ICM cells (Fig. S2D compared to S2F, p=0.13 Student Test or p=0.19 Chi2 Test respectively). In addition cells move in the ICM in both conditions (Fig. 3A-D compared to 3F). This microinjection approach has been used extensively to generate clones of labelled cells at post-implantation stages, showing that this method leads to normal development of the blastocyst into an egg cylinder.

Cell tracking

Images in the green-fluorescent channel were deconvolved using Huygens software. 4D cell tracking was performed using the software written in IDL (ITT Visual Information Solutions) (England et al., 2006). The centre of each ICM nucleus at each time point was manually defined. The lineage of cells was monitored at each cell division. To compensate for the global movements of the whole embryos during filming, the mean trajectory of all cell movements was subtracted from each individual cell trajectory, thus keeping the centre of gravity of the ICM fixed. All distances, including two sister cell separation when they first appear and the distance travelled by a cell, were calculated as the Cartesian straight-line distance between consecutive points. In some instances, the blastocoelic cavity was manually outlined on every z-section of the transmission channel at all time frames. The distance of a cell to the cavity was calculated as the shortest distance between the cell centroid and the closest vertex of a dense mesh representing the boundary of the cavity. 10 µm was taken as a cut off to distinguish deeper and surface cells at the start of imaging and 5µm at the end. Quicktime VR movies representing cells as spheres coloured according to their fate were generated in IDL and assembled using VR Worx (VR Toolbox, Inc). Blastocyst 2210_b5, which was a later stage and had many ICM cells, could not be tracked fully for more than 12 hours and therefore was not included in Tables 1-2.

Analysis of protrusions and velocities of GAP-RFP injected cells

These analyses were performed on z-projections of the maximum intensity of the red-channel. The centre of gravity (CG) of GAP-RFP-injected cells was measured in Metamorph software version 7.0 from Molecular Devices Corporation with the Integrate Morphometric Analysis function by thresholding z-projections. The coordinates were corrected for the movement of the embryo, by subtraction of the coordinates of the centre of gravity of the embryo. This centre of gravity was measured similarly by thresholding filtered z-projections of the maximum intensity of the green-channel. The position of the tip of the protrusions ($CGPX$; $CGPY$) was manually defined in Metamorph software. The travelled distance per cell and the angle between the protrusion and the trajectory were calculated in Excel software using a custom Macro. Briefly, the travelled distance of a cell between time point t and t+1 was calculated as $((CGX_t - CGX_{t+1})^2 + (CGY_t - CGY_{t+1})^2)$ with (CGX; CGY) the corrected coordinates of the centre of gravity of the cell. The conversion in µm is based on a resolution of 0.62 µm per pixel. The velocity of a cell is the mean velocity between every consecutive time points. The angle between the protrusion and the trajectory was calculated as $\alpha = Arccos((a + b - c) / (2 * a * b))$, where $a = (CGX_{t2} - CGX_{t1})^2 + (CGY_{t2} - CGY_{t1})^2$, $b = (CGX_{t1} - CGPX_{t1})^2 + (CGY_{t1} - CGPY_{t1})^2$ and $c = (CGX_{t2} - CGPX_{t1})^2 + (CGY_{t2} - CGPY_{t1})^2$. The trajectory was considered between time point t1, when the protrusion was observed, and t2, the nearest successive time point when the cell had moved significantly, with a minimal distance taken as 5 pixels. Radial bar graphs were drawn in Excel software using a custom Macro.

Computer modelling

Initialization—The model simulates the blastocyst ICM as an initial set of 14 cells, of which 7 are surface (position 1) and 7 deeper (position 2) cells. The gene expression state of these cells and of their subsequent daughters (which may be considered as the level of expression of specific PE or epiblast markers) is either indeterminate (state 3), PE (state 1) or epiblast (state 2). A fourth state (state 0) is defined for apoptotic cells. Initially, all cells are in state 3. Alternatively, they may be randomly allocated to any of the 3 gene expression states (i.e. 33% of cells in each state). This had no influence on the final score of the models.

Parameters—The model is probabilistic, so that there is a probability at each time step that a given cell will undergo any of the four behaviour. These probabilities are the parameters of the model:

- Experimental results have shown that all initial cells will divide during the first round, and half of the subsequent generation during the second round. The model thus only includes a stochastic allocation during those two rounds. However we defined a parameter for the probability that a given division will influence cell position. Division may either be symmetric or "horizontal" (the two daughter cells keep the same position as the mother cell), or asymmetric (one daughter ends up at the surface, the other in a deeper position). ProbaHorizDiv is the probability of "horizontal" division. Our observations gave a direct measurement of this parameter, which differs between the two rounds of divisions : ProbaHorizDiv1 = 0.55, ProbaHorizDiv2 = 0.87 (n1=40, n2=39). Our observations indicate that the percentage of symmetric divisions increases with time.

- The probability that a cell will undergo apoptosis at each time step is defined as **ProbaApoptosis**. In a Random model, apoptosis affects cells randomly. In a Cell sorting model, the probability of apoptosis is influenced by the gene expression state such that it is increased by a factor, **FactorApoptosis**, when the gene expression state of the cell is not congruent with its position (e.g. a surface cell expressing epiblast markers). Plusa et al (2008) have shown that a PDGFRα-GFP$^+$ cell in the deeper ICM is six times more likely to die than a GFP$^+$ cell at the surface, therefore FactorApoptosis is set at 6 for deeper cells with expression state 1. There is no experimental data for a potential increase of apoptosis of surface cells with expression state 2, therefore FactorApoptosis was set at 1 for this cell population. Alternatively, a symmetrical FactorApoptosis of 6 was tested (see text).

- Cell movement changes the position of a cell. In a Random model, there is equal probability that a cell will either change position or remain in its original position. In a Cell sorting model, cell movement is influenced by its gene expression state. If the gene expression state of a cell is congruent with its position (e.g. a surface cell expressing PE markers), the probability that the cell will move to the alternative position (deeper in this case) is lower than 0.5 : we call it WeakProbaVertMvmt. Conversely, if the gene expression state is not congruent with the position of the cell, the probability that the cell will move to the alternative position (deeper in this case) is higher than 0.5 and called StrongProbaVertMvmt. Both parameters were shown by Plusa et al. (2008) to vary with time, such that the efficiency of cell sorting improves with time. We assume that both parameters are linear functions of the number of sorted cells (with congruent gene expression and position), with an initial value of 0.50. This initial value is in agreement with Plusa et al. (2008). They measured the movement of PDGFRα-GFP$^+$ cells according to their initial position, both during the 32/64 and 64/128 cell transitions. When the two measurements are joined by a straight line, this intersects time = 0 (i.e. the start of the simulation which corresponds to the 32 cell stage blastocyst) at approximately 0.50. This indicates that there is no cell sorting initially. The probability of cell movement is thus simulated as :

$$\text{WeakProbaVertMvmt} = 0.50 - \textbf{SlopeWeakProbaVertMvmt} * X$$
$$\text{StrongProbaVertMvmt} = 0.50 + \textbf{SlopeStrongProbaVertMvmt} * X$$

where X is the number of sorted cells in the compartment. It is assumed that cell sorting has the same efficiency in both the surface and deeper compartments.

- The probability that a cell will change its gene expression state at any time step is the parameter **FreqDiff**. The allowed changes are shown in Fig. S3A. The probability of a given change is defined by a transition matrix, which includes the parameter **Induction** (**I**). In a Random model, all changes are equally probable and independent of cell position (**I** = 0.5). In an Induction model, the higher **I**, between 0.5 and 1, the stronger the influence of the cell position. The transition matrixes are given in Fig. S3B. The probability of a cell to change gene expression is the value read in the matrix times **FreqDiff**.

Model simulations—ICM development is simulated in four successive phases:

-Phase 1 is before the start of the first round of mitoses. Cells are only allowed to move and change gene expression. We assume that the start of the first round of divisions (**Round1start**) is determined stochastically: it is a normal random variable with mean = 4.5 hours and standard deviation = 4.5 hours (as determined experimentally).

-Phase 2 corresponds to the first round of mitoses and lasts 8.6 hours (as determined experimentally). Cells are allowed to move, change gene expression and divide.

-Phase 3 is between the two rounds of divisions and lasts 6.2 hours (as determined experimentally). This is when apoptosis has been shown to start experimentally. Cells no longer divide but are allowed to move, change gene expression or die.

-Phase 4 corresponds to the second round of mitoses and was simulated over 8h. Cells may move, change gene expression, divide and die.

-The simulation ends when 50% of the lineages have undergone the second round of mitoses (as determined experimentally). The total duration of the simulation was variable, between 20h and 34h with 96% probability.

The model simulates the 4 successive phases, by calculating at each time step and for each cell (uniquely identified by a number), the position (surface or deeper) and the gene expression state. The time step is taken as 2 hours, since our observations show that a typical cell will travel a distance equal to its own diameter within approximately 2h.

Output—Simulations are done for a sample of 7 different embryos and provide the following predicted values (mean and standard deviation) for each sample: A-number of dead daughter cells, B-number of surface daughter cells derived from an initial surface mother cell, which generates only surface daughter cells, C- number of deeper daughter cells derived from an initial surface mother cell, which generates only deeper daughter cells, D-number of surface daughter cells derived from an initial surface mother cell, which generates both surface and deeper daughter cells, E-number of deeper daughter cells derived from an initial surface mother cell, which generates both surface and deeper daughter cells, F-number of surface daughter cells derived from an initial deeper mother cell, which generates only surface daughter cells, G-number of deeper daughter cells derived from an initial deeper mother cell, which generates only deeper daughter cells, H-number of surface daughter cells derived from an initial deeper mother cell, which generates both surface and deeper daughter cells, I-number of deeper daughter cells derived from an initial deeper mother cell, which generates both surface and deeper daughter cells, J-number of cell lineages disappearing by apoptosis, K-number of cell lineages originating from the surface and generating only surface daughter cells, L-number of cell lineages originating from the surface and generating only deeper daughter cells, M-number of cell lineages originating from the surface and generating both surface and deeper daughter cells, N-number of cell lineages originating from the deeper ICM and generating only surface daughter cells, O-

number of cell lineages originating from the deeper ICM and generating only deeper daughter cells, P-number of cell lineages originating from the deeper ICM and generating both surface and deeper daughter cells, Q-number of mispositioned surface cells with gene expression state 2 (epiblast) at the end of the simulation, R-number of mispositioned deeper cells with gene expression state 1 (PE) at the end of the simulation, S-number of cells with gene expression state 3 (indeterminate) at the end of the simulation.

These 19 predicted values were compared to the observed values. The reference table of the observed values is shown in Fig. S3C. The results of the model were evaluated by the **score**= sum $(Pr_i – Obs_i)^2 / \sigma_i^2$, where Obs is the observed mean value of the ith term in the table in Fig. S3C, Pr_i is the mean value predicted by the model and σ_i^2 is the variance of the observed value. The smaller the score, the better the fit between the predicted and observed values and so the better the model.

Optimization of the free parameters—The value of the free parameters is optimized by minimizing the score. A Random model, is defined by 6 fixed parameters (**ProbaHorizDiv1**=0.55, **ProbaHorizDiv2**=0.87, **Induction**=0.5, **SlopeWeakProbaVertMvmt**=0, **SlopeStrongProbaVertMvmt**=0, **FactorApoptosis**=1) and 2 free parameters, optimized as follows : **FreqDiff**=1 and **ProbaApoptosis**=0.078.

In a Cell sorting model, there are 4 fixed parameters (**ProbaHorizDiv1**=0.55, **ProbaHorizDiv2**=0.87, **Induction**=0.5, **FactorApoptosis**=6) and 4 free parameters, optimized as follows : **FreqDiff**=1, **ProbaApoptosis**=0.05, **SlopeWeakProbaVertMvmt**=0.025, **SlopeStrongProbaVertMvmt**=0.023.

In an Induction model, there is an additional free parameter, optimized as **Induction**=1. In a Random + Induction model, the other free parameters are optimized as follows : **FreqDiff**=0.68 and **ProbaApoptosis**=0.122. In a Cell sorting + Induction model, the other free parameters are optimized as follows : **FreqDiff**=1, **ProbaApoptosis**=0.05, **SlopeWeakProbaVertMvmt**=0.022, **SlopeStrongProbaVertMvmt**=0.026.

As an increase in the number (k) of free parameters may in itself improve the score of a model, we validated the score differences between the models using the Akaike criterion (AICc =2k + n[ln{2π Score/n}+1]+2k(k+1)/(n-k-1) where n is the number of observations (=19)) : in a Random model AICc = 143 (k=2), in a Cell sorting model AICc = 145 (k=4), in a Random + Induction model AICc = 120 (k=3), in a Cell sorting + Induction model AICc = 76 (k=5). The lower AICc, which is indicative of the best fit model, is still the Cell sorting + Induction model.

Validation of the model—We validated the Cell sorting + Induction model, our best scored model. We first compared individually the 19 output values of a simulated sample with that of the observed sample. In a sample of 100 simulated series of 7 embryos, the output values were in the confidence interval at 95% of the observed values in all cases but one (value S). In addition, we compared statistically significant patterns of the experimental sample:

-In our experimental sample, the number of unipotent lineages (K+L+N+O=50 or mean 7.1 ± 3.1 per embryo) is almost twice the number of bipotent lineages (M+P= 27 or mean 3.9 ± 1.3 per embryo) and this difference is statistically significant (Student test, p = 0.025). In a sample of 100 simulated series of 7 embryos, the average number of unipotent lineages is 8.6 ± 0.9 per embryo, against 4.2 ± 0.7 bipotent lineages.

-In our experimental sample, the number of surface daughter cells originating from surface progenitors (B+ D=61, i.e. 8.7 ± 3 per embryo) is larger than the number of deeper daughter cells originating from surface progenitors (C+ E=40, i.e. 5.7 ± 2.1 per embryo), and this difference is significant (Student test, p = 0.003). In a sample of 100 simulated series of 7 embryos, the average number of surface daughters from surface progenitors is 7.2 ± 1.2 per embryo, against 6.5 ± 1.3 deeper daughters from surface progenitors.

-In the experiments carried out by Plusa et al. (2008), cell sorting was measured during two phases. During the 32/64 cell transition (Phase 2 in our model), 72% of surface cells expressing a PE marker remain at the surface, whereas this proportion increases to 100% during the 64/80 cell transition (Phase 4 in our model). Conversely, the proportion of deeper (mispositioned) cells expressing the PE marker and remaining in a deeper position decreases from 34% to 16%. In a sample of 100 simulated series of 7 embryos, the average proportion of surface cells with expression state 1 remaining at the surface during Phase 2 is 90% and this proportion increases to 100% during Phase 4. Conversely, the proportion of deeper cells with expression state 1 decreases from 28% to 0%.

These simulated patterns were in the confidence interval at 95% of the observed patterns in all cases but one (the proportion of deeper cells with expression state 1 and remaining deeper in Phase 4). Taken together, these data validate our model as reproducing most features of blastocyst development. The 2 simulated values (out of 27) which are outside the confidence interval of the observed values, indicate that our model does not permit enough mispositioned cells and is too tolerant with indeterminate cells.

Results and Discussion

Behaviour of all ICM cells

To follow the lineages and dynamics of ICM cells, we tracked cells simultaneously in 4D as the blastocyst develops to the stage when the PE forms. Time-lapse images of embryos were acquired in multiple optical sections, similarly to our earlier studies (Bischoff et al., 2008), using H2B-GFP mice (Hadjantonakis and Papaioannou, 2004). We first confirmed that such imaged embryos could develop normally (Fig. S1A-E). We also verified that the movement of nuclei within ICM cells is negligible, as cells are small and occupied at 26% by their nucleus (sd=6%, n=266). In cells injected with the membrane localised GAP-RFP, the movement of the cell and that of its nucleus were analysed separately and found to be parallel (Fig. 1F, n=5). Therefore tracking nuclei of ICM cells is a reliable indication of cell movements.

Tracking all ICM cells simultaneously revealed extensive cell division within the ICM, in both deeper and surface cells (Fig. S2A). During 20-30 h of imaging, cells of all lineages divided at least once and almost 50% went through two rounds of division, such that by the end of the imaging session, one lineage usually corresponded to 3-4 cells. Interestingly, cell division occurred in waves with an average of 15h between the sixth and seventh cleavages (Fig. S2B-D). After the completion of the sixth cleavage, on average 25% of daughter cells underwent apoptosis (Fig. S2D-E), such that some ICM lineages did not generate any progeny. Later apoptosis is consistent with previous studies on fixed embryos (Copp, 1978; Handyside and Hunter, 1986).

Our time-lapse studies revealed that individual cells move at an average velocity of 0.11μm/min (sd=0.02, n=69). Individual trajectories of cells appeared convoluted, indicating that cells exchange positions (Fig. 1A and F, movie Fig1video1). This movement seemed uniform, meaning we could not distinguish any particular population of ICM cells that had a distinct behaviour in terms of movement velocity (Fig. 1B).

We considered that several mechanisms might cause cell movement within the ICM. It may be a passive rearrangement of cells. When a dividing cell rounded at metaphase, neighbours were pushed away (Fig. 1C1). In contrast, when sister nuclei separated after anaphase, neighbours occupied the space in between the daughters (Fig. 1C2). To analyse the movement generated by cell division, we measured the distance between the nuclei of daughter cells at anaphase and found that it was, on average, 17μm (n=83, sd=4). This was lower than the maximum displacement of a cell from its starting point (27μm). Therefore movement triggered by cell division seemed insufficient to explain the distance travelled by cells and suggested that active movement might also be involved. To examine this possibility, we first followed the shape of cells, as active movement is known to be associated with the formation of cell protrusions. This revealed that ICM cells can change shape very dynamically (Fig. 1D, movie Fig1video2), having many filopodia, which were fine and short (average length 5.6μm, n=31, sd=2.4, Fig. 1D1) and less frequently broader protrusions that correspond to lamellipodia (Fig. 1D2, frames 8h50-9h20). These protrusions were mainly oriented within 90° in the direction of movement (Fig. 1E), as though cells were exploring their environment. Thus individual ICM cells move extensively and their movements appear to involve both passive and active mechanisms.

Actin-dependent cell movement

To explore whether the microtubule and/or actin networks could be important for ICM cell movement we tracked movements of cells in the presence of specific inhibitors. To disrupt microtubules, we used nocodazole (Fig. 2A-B; the actin network, as revealed by phalloidin staining, was unperturbed by this treatment). To disrupt actin, we employed cytochalasin D (Fig. 2C), which did not affect nuclear division, showing that the microtubule network was functional.

In the presence of nocodazole, movements of cells were still extensive with dynamic shape changes and projection of filopodia (Fig. 2D-F, movie Fig2video1 and 2). In contrast, in the presence of cytochalasin D, cell movement was dramatically reduced (Fig. 2F-G, movie Fig2video3). Cells rounded but otherwise did not change shape, in contrast to control embryos (Fig. 2H, movie Fig2video4). No dynamic protrusions were projected and membrane blebs formed, a well-known effect of cytochalasin D.

Thus, it appears that although some of the ICM cell movement is passive, the majority of cell movement is active and involves actin. This active cell movement is compatible with both cell migration and cell intercalation and could contribute to sorting of cell lineages.

Movement of cells between the surface and deeper compartments of the ICM

Given such extensive movement of ICM cells, we wondered to which extent this affected the position of cells in the surface and deeper compartments of the ICM, which ultimately will be colonised by distinct cell lineages. To address this question we either injected single ICM cells with a lineage marker and followed its movement and final position (Fig. 3A-D) or we fully tracked the positions of all ICM nuclei in single embryos and measured the distance of nuclei to the cavity over time, as an objective indication of their position (Fig. 3E-F). These observations revealed all possible configurations. Some cells kept their position during blastocyst development, either on the surface throughout the movie (Fig. 3A and 3F9, movie Fig3video1), or deeper (Fig. 3C and 3F cell 2b, supplemental movie Fig3video3). Other cells changed compartments, from the surface deeper (Fig. 3B and 3F6, supplemental movie Fig3video2) or from the deeper ICM towards the surface (Fig. 3D and 3F1, supplemental movie Fig3video4). In addition to active cell movements (Fig. 1D2), we observed asymmetric divisions leading to a change of compartment (asterisks in Fig. 3F). Some cells appeared to change compartment more than once (cell 5a changed twice, cell 1b

three times in Fig. 3F) and this did not occur only at early stages of ICM development, but also after 25h of imaging (for example cell 1a, 7ba or 12ab). These results indicate that there is an exchange of cells between the surface and deeper ICM compartments until relatively late in the development of the blastocyst. We acknowledge that although tracking nuclei of ICM cells is a reliable indication of cell movements (Fig. 1F), we cannot exclude the possibility that in some cases, the periphery of a deeper cell may make some contribution to the surface layer. Our approach allowed us to track all ICM cells, irrespective of their gene expression. When cell movement and gene expression were followed together, it was shown that cells maintaining expression of the PE marker PDGFRα have a net movement towards the cavity (Plusa et al., 2008), indicative of cell sorting. However the fluctuation of the expression of PE or epiblast markers and our observations that not all ICM cell movements appears unidirectional suggests that positional induction might also be involved in addition to cell sorting to achieve segregation of ICM lineages.

Early and late clonal segregation of ICM cell lineages

As ICM cells can change positions, we examined to which extent the PE derives from cells initially at the surface of the early ICM. The analysis of all tracked cell lineages revealed that 59% of the cells on the surface of the late ICM were derived from a mother cell already at the surface at the early blastocyst stage (Table 1, 121 cells in 7 tracked blastocysts). This is an average, as we observed biological variation between individual embryos. In 41% of cases, surface cells were derived from the initial deeper compartment, indicating that at least some lineage precursor cells are initially intermingled in the early ICM. This supports the idea that the ICM cell population is heterogeneous, as indicated by the "salt and pepper" expression patterns of PE and epiblast markers (Chazaud et al., 2006; Plusa et al., 2008) or gene expression profiling in ICM (Kurimoto et al., 2006) or ES cells (Stewart et al., 2006; Singh et al., 2007).

Because we were able to track for the first time all ICM cells, we could also determine whether the segregation between epiblast and PE lineages has been already completed in the early ICM. We found that many individual ICM lineages (6 to 10, Table 1) contributed to the surface by the end of the imaging session. However, only half of these lineages contributed exclusively to the surface, irrespective of their origin in the early ICM. Overall in the 77 tracked lineages, we found that two thirds of early ICM cells had a restricted contribution to either the surface or the deeper compartment of the late ICM (Table 2, for example surface lineages 1 and 9 or deeper lineage 6 in Fig. 3F), whereas one third of the lineages is bipotent and contribute to both ICM compartments (for example lineage 5 in Fig. 3F or see 3C-D). Although such bipotent PE and epiblast cells had been detected previously (Gardner, 1983; Rossant, 1984; Weber et al., 1999; Chazaud et al., 2006; Perea-Gomez et al., 2007), the extent of this phenomenon was unclear, as the potential of all cells from a single ICM could not be analysed.

This analysis of lineages of all ICM cells indicate that allocation of cells to the epiblast and PE lineages is a continuous process, which is not completed in the early ICM. This is consistent with observations that at early blastocyst stage *Gata6*-enriched cells are not totally devoid of *Nanog* expression and vice-versa (Kurimoto et al., 2006; Singh et al., 2007; Plusa et al., 2008). Thus, our results suggest that the segregation between epiblast and PE lineages is not completed at the early blastocyst stage.

Gata6 is necessary but not sufficient for the positioning of cells at the ICM surface

Since our results demonstrated movement of ICM cells between surface and deeper positions, we wished to understand whether expression of some key PE markers, such as *Gata6*, could be sufficient to sort cells. In addition to *Gata6*, we examined a possible role of

Nr2f1 (also known as *COUP-TFI*). This is because it is already expressed at the surface of the ICM at E3.5 (Murray and Edgar, 2001), in contrast to the mosaic expression of *Gata6*. We also wondered whether the canonical *Wnt9A*, shown to be specific to the surface of the ICM from the time of cavitation, could be a candidate in signalling surface identity to ICM cells (Person et al., 2005, Kemp et al., 2005). We examined whether expression of these genes is sufficient to drive deeper cells to the surface, or whether interfering with the function of these markers can maintain surface cells in this position.

We microinjected individual ICM cells with synthetic mRNA, to induce over-expression or expression of dominant-negative forms of these factors (Fig. 4A). To monitor the descendants of these cells by time-lapse microscopy, they were co-injected with a cell marker (RFP) that did not perturb their fate (see Material and Methods). We first injected control embryos with these constructs to show that they were functional (Fig. 4B-E). Our control experiments also revealed that Gata6 and Nr2f1 do not affect ICM cell proliferation or survival, whereas Wnt9A promotes both (Fig. S2F).

We analysed the distribution of the progeny of cells which were injected at the surface of the early ICM. This revealed that in the presence of dominant-negative Gata6, ICM cells contributed significantly less to the surface of the late ICM, and thus to PE (6% compared with 40% in control, Fig. 4F), i.e. they contributed more to the epiblast. In contrast, injection of dominant-negative forms of either Nr2f1 or Wnt9A, did not change the distribution of cells. These results indicate that Gata6 is important for maintaining cells at the surface of the ICM.

We therefore wondered whether providing higher levels of Gata6 in deeper cells, might cause these cells to sort in agreement with an earlier hypothesis (Chazaud et al., 2006). However, we did not observe this: over-expression of *Gata6* in deeper ICM cells did not significantly change their location (Fig. 4G). This is in agreement with the finding that deeper layers of embryoid bodies derived from ES cells over-expressing *Gata6* do not differentiate into endoderm (Fujikura et al., 2002). However, interestingly a combination of *Gata6* and *Wnt9A* in deeper ICM cells was enough to significantly re-position cells to the surface (27% of deeper fate compared with 66% in control), whereas the sole overexpression of *Wnt9A* had no significant effect.

These results suggest that while Gata6 expression in deeper cells on its own cannot drive cells to change their position, a combination of Gata6 with an additional signal, such as Wnt9A, could be sufficient to drive cells to the surface ICM. It is possible that other Wnts expressed in the blastocyst could also contribute to this process, although thus far only Wnt9A was shown to distinguish between the surface and deeper ICM (Kemp et al., 2005). Although Wnt9A is a signalling molecule and therefore could have a non cell-autonomous effect, Wnt9A may also act as a stabiliser of gene expression as proposed in other systems (Martinez Arias, 2000).

Cell sorting and positional induction are both necessary to achieve segregation of epiblast and PE lineages

To further investigate the involvement of cell sorting or random movements and positional induction of fate during the segregation of epiblast and PE lineages, we have used computer modelling. We designed a cellular automaton model to simulate the development of the ICM in similar conditions to our time-lapse observations. Each cell is defined by its position (surface, deep) and its gene expression state (epiblast markers, PE markers, indeterminate state). The model is probabilistic, so that there is a probability at each time step that a given cell would undergo cell division, apoptosis, cell movement and/or gene expression change (Fig. S3A-B). The results of the model were evaluated by a score (the lower the better)

which compares a set of 19 values in simulated versus experimental conditions (Fig. S3C), including lineage data, the rate of apoptosis and the number of mispositioned (gene expression state and position are not congruent as for example deeper cells expressing PE markers) or indeterminate cells. Several hypotheses were tested (see Materials and Methods for more detail). In a Random model, cell movement and apoptosis were independent of the gene expression state of the cell. In contrast, in a Cell sorting model both parameters were dependent on gene expression : mispositioned cells are more likely to die or move. We found that in either Random or Cell sorting model, the score was poor (Fig. 5A-B). Therefore we added a mechanism of positional induction. In an Induction model, the gene expression state depends on the position of a cell : if the gene expression state is congruent with the position of a cell, it is less likely to change (stable gene expression). When Induction was added to the Random model, the score was improved. However, the improvement was even better when Induction was added to the Cell sorting model (Fig. 5C). Therefore the Cell sorting model coupled to Induction provided the best fit to the observed data.

Selective apoptosis is known to exist in the ICM as cells expressing the PE marker PDGFRα are more likely to die when positioned in the deeper compared to the surface ICM (Plusa et al., 2008). It was proposed that selective apoptosis might enhance lineage segregation, but it had not been tested. We have addressed this issue in our simulations. In a Cell Sorting model, the absence of selective apoptosis undermined the score (Fig. 5D1 compared to B). Experimentally, it has only been shown that deeper cells expressing PE markers are more likely to die. If we considered that symmetrically, surface cells expressing epiblast markers were also more likely to die, with the same factor of increase, then the score of the Cell Sorting model was slightly improved (score=201±50, Student Test p<0.001 compared to Fig. 5B). However, selective apoptosis was worse than induction for improving the score (201±50 compared to 18±10). In a Cell Sorting + Induction model, neither the absence of selective apoptosis (Fig. 5D2), nor a symmetrical selective apoptosis for both mispositioned populations (score=25±12) significantly influenced the score (compared to Fig. 5C2). Thus selective apoptosis of cells mispositioned relative to their gene expression does not appear to be a critical factor to enhance ICM lineage segregation.

The mechanism of cell sorting remains speculative. It was shown to increase with time (Plusa et al., 2008) and we assumed here that the strength of cell sorting increases with the number of sorted cells. Alternative ways of varying cell sorting with time might further improve the score of the model.

Our simulations support the view that both cell sorting movements and positional induction contribute to the segregation of ICM lineages. We found that the induction needs to be strong (maximum probability), i.e. once the gene expression state is congruent with the position of the cell, it becomes fixed. A slight decrease of the induction had a major impact on the score. Variation of the induction in time, such that it increased gradually, did not change the final state and thus the score, but the way it was reached : at the time when induction got maximum, the ICM became mostly composed of sorted cells (with congruent gene expression state and position). Experimental data indicate that a few mispositioned cells are still present at the end point, in contrast to our best simulations. Therefore an additional mechanism which modulates induction seems to be required.

Taken together, our data suggest that the formation of the PE involves active, actin-dependent movement of cells, but also induction of fate depending on cell position (Fig. 5E). It appears that a proportion of cells change their position in the ICM until the right cells get trapped in a compartment and induced to differentiate. Wnt9A is a candidate to play a role in this stabilisation, as Wnts have been proposed to stabilise gene expression (Martinez Arias,

2000). Other aspects of stabilisation are likely to include cell polarisation (Gerbe et al., 2008) and changes in cell adhesion (Liu et al., 2009). The composite mechanism of PE formation that we characterise creates a flexible environment, compatible with the well-known plasticity of early ICM cells, in which gene fluctuation and cell movement can compensate for cell addition or loss.

Supplementary Material

Refer to Web version on PubMed Central for supplementary material.

Acknowledgments

References

Adam F, Sourisseau T, Metivier R, Le Page Y, Desbois C, Michel D, Salbert G. COUP-TFI (chicken ovalbumin upstream promoter-transcription factor I) regulates cell migration and axogenesis in differentiating P19 embryonal carcinoma cells. Mol Endocrinol. 2000; 14:1918–33. [PubMed: 11117523]

Bischoff M, Parfitt DE, Zernicka-Goetz M. Formation of the embryonic-abembryonic axis of the mouse blastocyst: relationships between orientation of early cleavage divisions and pattern of symmetric/asymmetric divisions. Development. 2008; 135:953–62. [PubMed: 18234722]

Campbell RE, Tour O, Palmer AE, Steinbach PA, Baird GS, Zacharias DA, Tsien RY. A monomeric red fluorescent protein. Proc Natl Acad Sci U S A. 2002; 99:7877–82. [PubMed: 12060735]

Chambers I, Silva J, Colby D, Nichols J, Nijmeijer B, Robertson M, Vrana J, Jones K, Grotewold L, Smith A. Nanog safeguards pluripotency and mediates germline development. Nature. 2007; 450:1230–4. [PubMed: 18097409]

Chazaud C, Yamanaka Y, Pawson T, Rossant J. Early Lineage Segregation between Epiblast and Primitive Endoderm in Mouse Blastocysts through the Grb2-MAPK Pathway. Dev Cell. 2006; 10:615–24. [PubMed: 16678776]

Copp AJ. Interaction between inner cell mass and trophectoderm of the mouse blastocyst. I. A study of cellular proliferation. J Embryol Exp Morphol. 1978; 48:109–25. [PubMed: 744943]

England SJ, Blanchard GB, Mahadevan L, Adams RJ. A dynamic fate map of the forebrain shows how vertebrate eyes form and explains two causes of cyclopia. Development. 2006; 133:4613–7. [PubMed: 17079266]

Fujikura J, Yamato E, Yonemura S, Hosoda K, Masui S, Nakao K, Miyazaki Ji J, Niwa H. Differentiation of embryonic stem cells is induced by GATA factors. Genes Dev. 2002; 16:784–9. [PubMed: 11937486]

Gardner RL. Origin and differentiation of extraembryonic tissues in the mouse. Int Rev Exp Pathol. 1983; 24:63–133. [PubMed: 6302028]

Gardner RL, Rossant J. Investigation of the fate of 4-5 day post-coitum mouse inner cell mass cells by blastocyst injection. J Embryol Exp Morphol. 1979; 52:141–52. [PubMed: 521746]

Gerbe F, Cox B, Rossant J, Chazaud C. Dynamic expression of Lrp2 pathway members reveals progressive epithelial differentiation of primitive endoderm in mouse blastocyst. Dev Biol. 2008; 313:594–602. [PubMed: 18083160]

Hadjantonakis AK, Papaioannou VE. Dynamic in vivo imaging and cell tracking using a histone fluorescent protein fusion in mice. BMC Biotechnol. 2004; 4:33. [PubMed: 15619330]

Handyside AH, Hunter S. Cell division and death in the mouse blastocyst before implantation. Roux's Archives of Developmental Biology. 1986; 195:519–526.

Hoppler S, Brown JD, Moon RT. Expression of a dominant-negative Wnt blocks induction of MyoD in Xenopus embryos. Genes Dev. 1996; 10:2805–17. [PubMed: 8946920]

Kemp C, Willems E, Abdo S, Lambiv L, Leyns L. Expression of all Wnt genes and their secreted antagonists during mouse blastocyst and postimplantation development. Dev Dyn. 2005; 233:1064–75. [PubMed: 15880404]

Koutsourakis M, Langeveld A, Patient R, Beddington R, Grosveld F. The transcription factor GATA6 is essential for early extraembryonic development. Development. 1999; 126:723–32.

Kuo CT, Morrisey EE, Anandappa R, Sigrist K, Lu MM, Parmacek MS, Soudais C, Leiden JM. GATA4 transcription factor is required for ventral morphogenesis and heart tube formation. Genes Dev. 1997; 11:1048–60. [PubMed: 9136932]

Kurimoto K, Yabuta Y, Ohinata Y, Ono Y, Uno KD, Yamada RG, Ueda HR, Saitou M. An improved single-cell cDNA amplification method for efficient high-density oligonucleotide microarray analysis. Nucleic Acids Res. 2006; 34:e42. [PubMed: 16547197]

Lemaire P, Garrett N, Gurdon JB. Expression cloning of Siamois, a Xenopus homeobox gene expressed in dorsal-vegetal cells of blastulae and able to induce a complete secondary axis. Cell. 1995; 81:85–94. [PubMed: 7720076]

Liang Q, De Windt LJ, Witt SA, Kimball TR, Markham BE, Molkentin JD. The transcription factors GATA4 and GATA6 regulate cardiomyocyte hypertrophy in vitro and in vivo. J Biol Chem. 2001; 276:30245–53. [PubMed: 11356841]

Liu J, He X, Corbett SA, Lowry SF, Graham AM, Fassler R, Li S. Integrins are required for the differentiation of visceral endoderm. J Cell Sci. 2009; 122:233–42. [PubMed: 19118216]

Martinez Arias A. The informational content of gradients of Wnt proteins. Sci STKE. 2000; 2000:PE1. [PubMed: 11752600]

Molkentin JD, Lin Q, Duncan SA, Olson EN. Requirement of the transcription factor GATA4 for heart tube formation and ventral morphogenesis. Genes Dev. 1997; 11:1061–72. [PubMed: 9136933]

Moriyoshi K, Richards LJ, Akazawa C, O'Leary DD, Nakanishi S. Labeling neural cells using adenoviral gene transfer of membrane-targeted GFP. Neuron. 1996; 16:255–60. [PubMed: 8789941]

Morrisey EE, Tang Z, Sigrist K, Lu MM, Jiang F, Ip HS, Parmacek MS. GATA6 regulates HNF4 and is required for differentiation of visceral endoderm in the mouse embryo. Genes Dev. 1998; 12:3579–90. [PubMed: 9832509]

Murray P, Edgar D. Regulation of laminin and COUP-TF expression in extraembryonic endodermal cells. Mech Dev. 2001; 101:213–5. [PubMed: 11231078]

Murray P, Edgar D. The topographical regulation of embryonic stem cell differentiation. Philos Trans R Soc Lond B Biol Sci. 2004; 359:1009–20. [PubMed: 15306413]

Nadijcka M, Hillman N. Ultrastructural studies of the mouse blastocyst substages. J Embryol Exp Morphol. 1974; 32:675–95. [PubMed: 4463224]

Perea-Gomez A, Meilhac SM, Piotrowska-Nitsche K, Gray D, Collignon J, Zernicka-Goetz M. Regionalisation of the mouse visceral endoderm as the blastocyst transforms into the egg cylinder. BMC Dev Biol. 2007; 7:96. [PubMed: 17705827]

Person AD, Garriock RJ, Krieg PA, Runyan RB, Klewer SE. Frzb modulates Wnt-9a-mediated beta-catenin signaling during avian atrioventricular cardiac cushion development. Dev Biol. 2005; 278:35–48. [PubMed: 15649459]

Plusa B, Piliszek A, Frankenberg S, Artus J, Hadjantonakis AK. Distinct sequential cell behaviours direct primitive endoderm formation in the mouse blastocyst. Development. 2008; 135:3081–91. [PubMed: 18725515]

Rossant J. Investigation of the determinative state of the mouse inner cell mass. II. The fate of isolated inner cell masses transferred to the oviduct. J Embryol Exp Morphol. 1975; 33:991–1001. [PubMed: 1176885]

Rossant, J. Somatic cell lineages in mammalian chimeras. In: Le Douarin, N.; McLaren, A., editors. Chimeras in developmental biology. Academic Press; New York: 1984. p. 89-109.

Singh AM, Hamazaki T, Hankowski KE, Terada N. A heterogeneous expression pattern for Nanog in embryonic stem cells. Stem Cells. 2007; 25:2534–42. [PubMed: 17615266]

Stewart MH, Bosse M, Chadwick K, Menendez P, Bendall SC, Bhatia M. Clonal isolation of hESCs reveals heterogeneity within the pluripotent stem cell compartment. Nat Methods. 2006; 3:807–15. [PubMed: 16990813]

Sutherland AE, Speed TP, Calarco PG. Inner cell allocation in the mouse morula: the role of oriented division during fourth cleavage. Dev Biol. 1990; 137:13–25. [PubMed: 2295360]

Tada M, Smith JC. Xwnt11 is a target of Xenopus Brachyury: regulation of gastrulation movements via Dishevelled, but not through the canonical Wnt pathway. Development. 2000; 127:2227–38. [PubMed: 10769246]

Torres-Padilla ME, Zernicka-Goetz M. Role of TIF1alpha as a modulator of embryonic transcription in the mouse zygote. J Cell Biol. 2006; 174:329–38. [PubMed: 16880268]

Weber RJ, Pedersen RA, Wianny F, Evans MJ, Zernicka-Goetz M. Polarity of the mouse embryo is anticipated before implantation. Development. 1999; 126:5591–8. [PubMed: 10572036]

Yang H, Lu MM, Zhang L, Whitsett JA, Morrisey EE. GATA6 regulates differentiation of distal lung epithelium. Development. 2002; 129:2233–46. [PubMed: 11959831]

Zernicka-Goetz M, Pines J, McLean Hunter S, Dixon JP, Siemering KR, Haseloff J, Evans MJ. Following cell fate in the living mouse embryo. Development. 1997; 124:1133–7. [PubMed: 9102300]

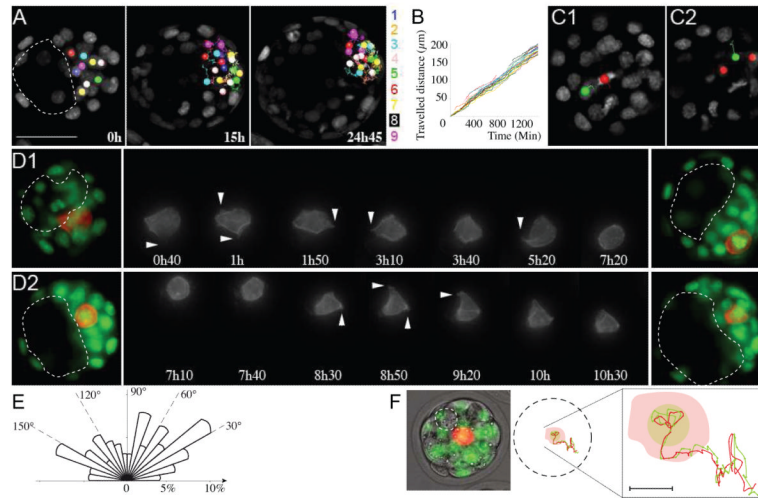**Figure 1. Cell movement in the ICM**

(A) Trajectories of ICM cells in an H2B-EGFP blastocyst. Each lineage is coloured and numbered. Time from the start of imaging is indicated. The position of the blastocoel is highlighted by a dashed white line. Scale bar 50μm. (B) In a typical tracked blastocyst, the cumulative distance travelled by each cell over time is represented, using a colour per cell. (C) Mitosis (red cell) results in movement of neighbouring cells (in green with its trajectory). An example of metaphase and anaphase are shown in C1 and C2 respectively. (D) Injection of membrane-localised GAP-RFP (red) reveals protrusions (arrowheads) of moving ICM cells. (E) The orientation of 163 protrusions from 14 cells was calculated in relation to the trajectory of the cell (x axis). The frequency of observations of the angular sectors is represented by the length of the sector. (F) Comparative trajectories of the centre of gravity of the cell (red) and that of its nucleus (green). On the left, the embryo is shown at the start of imaging. In the middle, the cell (pale red), its nucleus (pale green) and their respective parallel trajectories are represented at the scale of the embryo (dashed black line). On the right, a close-up is shown, with a scale bar of 10μm.
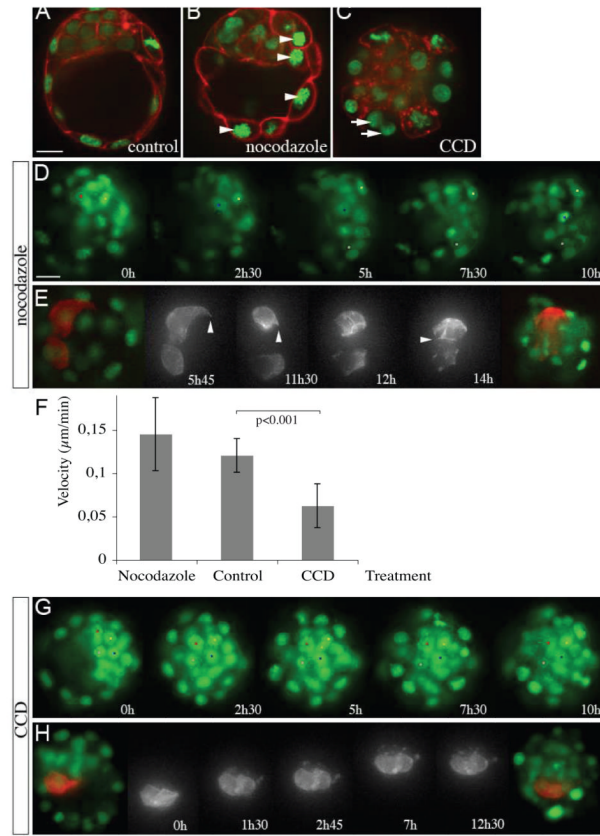
Figure 2. Effect of actin and microtubule inhibitors on ICM cell movement
(A-C) H2B- EGFP blastocysts stained with phalloidin (red) after 8-9h of control culture (A), or nocodazole (B) or cytochalasin D (C) treatment. Disruption of microtubules with nocodazole arrests cells in metaphase (arrowheads). Disruption of actin with CCD inhibits cytokinesis (arrows) and collapses the blastocoel. (D, G) In a typical imaging session, four cells have been tracked to show the persistence (D) or inhibition (G) of cell movement. (E, H) In GAP-RFP+ cells, protrusions (arrowheads) persist (C) or disappear (H) after drug treatment. (F) Velocities of GAP-RFP+ cells in control, nocodazole and CCD treated embryos. The mean value is shown for 9 (nocodazole, CCD) or 13 (GAP-RFP) cells, and the standard deviation as error bars. The mean cell velocity is significantly decreased after CCD treatment compared to control (nested ANOVA). Scale bar 20μm.
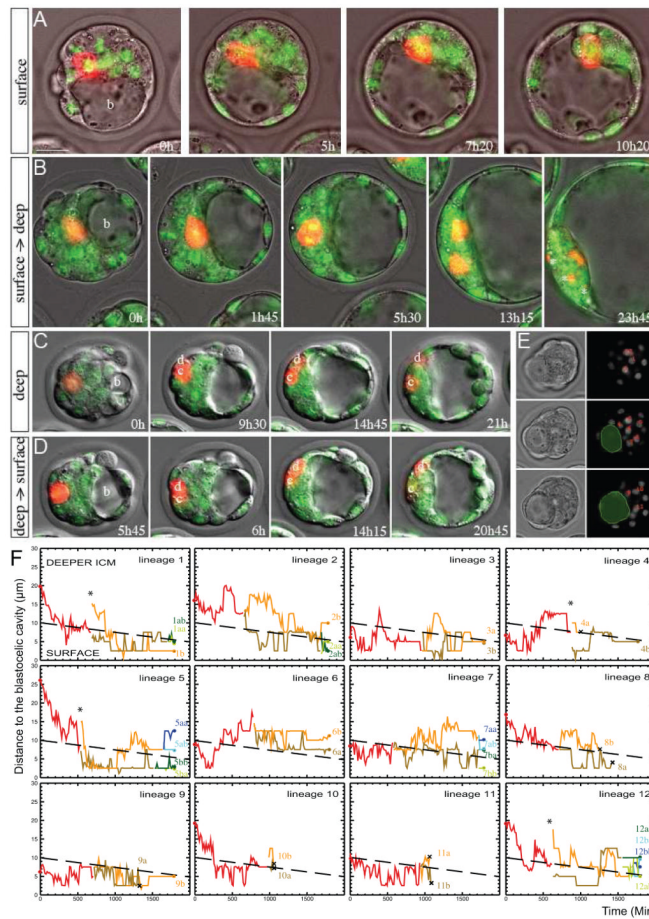
Figure 3. Exchange of cells between the surface and deeper ICM compartments

(A) The GAP-RFP[+] surface cell kept its position throughout the movie. b, blastocoel. (B) The RFP[+] surface cell reached the deeper layers of the ICM by active cell movement. After division, it gave rise to one deeper daughter cell, which died (apoptotic debris, asterisk), whereas the other daughter cell moved back to the surface and divided. (C-D) The RFP[+] deeper cell divided to give rise to a daughter cell (c) that remained deeper (C). The other daughter cell (d) moved to the surface (D). Two distinct z planes shown in C and D focus on each sister cell. Scale bar 25μm. (E) The blastocoel was traced in each z-plane of the transmission channel (left panels) ; its contour is shown in green in the green-channel images (right panels). (F) The shortest distance of each nucleus to the cavity is plotted over time. For each lineage, the initial cell is represented in red, the first generation in orange and brown and the second in dark and light blue and dark and light green. There was a general trend towards a decrease of the distance to the cavity, as the cavity expanded and the ICM was more compressed. A dotted black line estimates the limit between the two compartments over time. asterisks : asymmetric divisions leading to the separation of sister cells in two different compartments ; black crosses : apoptoses.
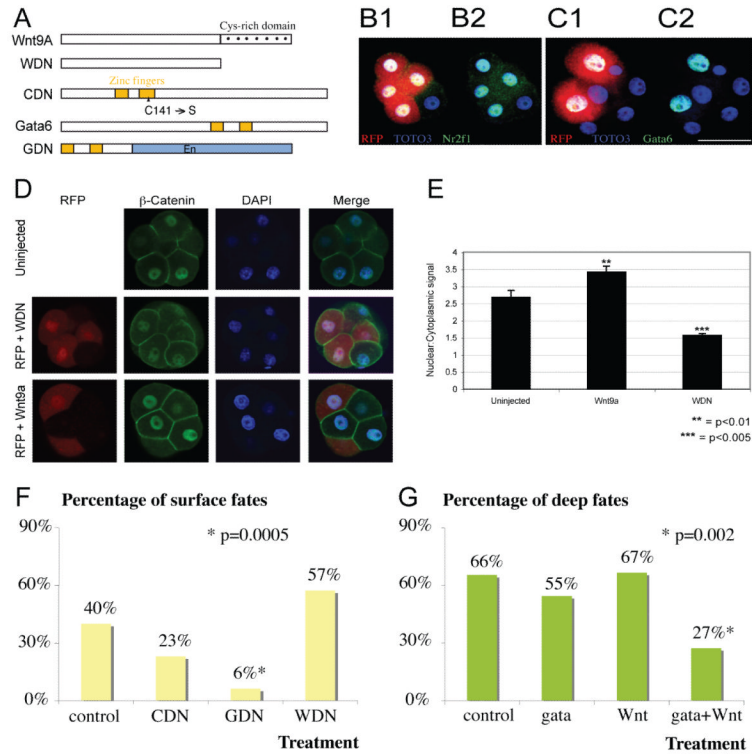
Figure 4. Molecular regulation of cell behaviour

(A) Schematic representation of the constructs used. WDN is a dominant-negative of Wnt9A, deleted for the C-terminal cysteine-rich domain. CDN is a dominant-negative of Nr2f1 (also known as COUP-TFI), with a point mutation in the DNA binding domain (orange). GDN is a dominant-negative of Gata6 in which the Gata6 DNA binding domain is fused to the engrailed (En) inhibitory transactivator domain. (B-D) Control embryos (8-cell stage) cultured for a day after single cell injection of RFP (red) at the 2-cell-stage. After co-injection with *CDN* (B) or *Gata6* (C) mRNA, immunostaining of Nr2f1 (B) or Gata6 (C) is detectable in the nuclei of RFP-positive cells, as expected. Three- (B1-C1) or two- (B2-C2) channel merged pictures. Scale bar 50μm. β-catenin localisation (D) in uninjected, WDN and Wnt9a injected embryos (8-cell stage). (E) The ratio between nuclear and cytoplasmic β-catenin (n=8 cells) is significantly decreased and increased after WDN and Wnt9A injection respectively (T- test). (F-G) Cells were injected at the blastocyst stage with RFP mRNA only (control) or together with one of the constructs shown in (A). Analysis of the fate of surface (F) and deeper (G) injected ICM cells, as a percentage of daughter cells observed at the end of the track at the surface and in the deeper compartment respectively. (*) The fate of GDN injected cells (Fisher test) and that of gata+Wnt injected cells are highly significantly different from the control. The numbers of daughter cells analysed are: 60 (surface control), 13 (CDN), 33 (GDN), 7 (WDN), 29 (deep control), 33 (gata), 6 (Wnt), 44 (gata+Wnt).
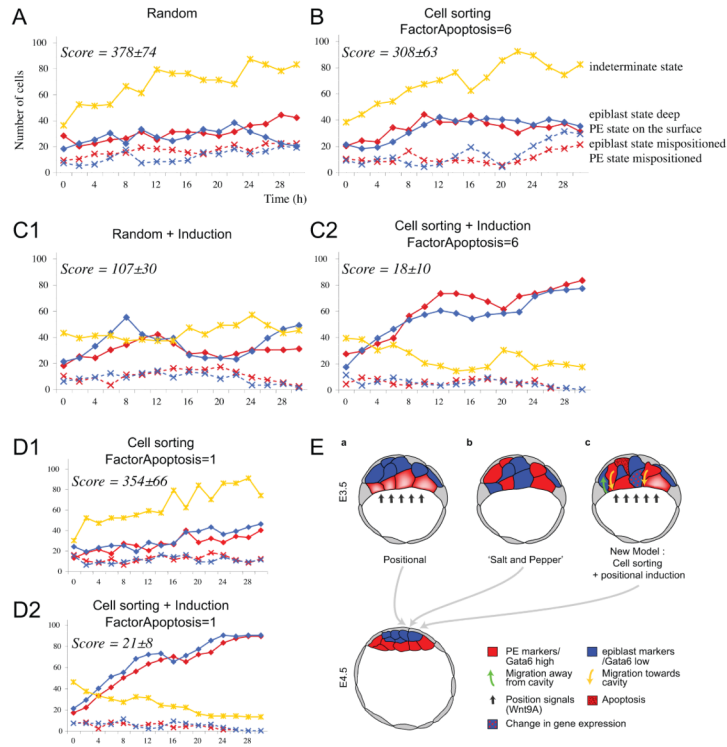
Figure 5. Computer modelling of lineage segregation

(A-D) The number of cells and score of each model are shown as the sum of 7 independent simulations. The number of cells with a given gene expression state (PE markers- red, epiblast markers- blue, indeterminate- yellow) is represented over time. straight line : sorted cells (with congruent gene expression state and position); dashed line : mispositioned cells. (A) Random model (equal probability). (B) Cell sorting model. If the gene expression state is congruent with the position of a cell, the probability that the cell will move to the alternative position is lower than 0.5. Conversely, if cells are mispositioned, the probabilities of movement and apoptosis are increased. (C) Induction model. If the gene expression state is congruent with the position of a cell it is less likely to change (i.e. stable gene expression). (D) In the absence of selective apoptosis of mispositioned cells the score of the Cell sorting model is significantly improved (D1 compared to B, $p<0.001$ Student test), but not that of the Cell sorting + Induction model (D2 compared to C2). (E) Theoretical models of PE formation. (a) Position-based model: cells in contact with the blastocoel cavity receive inducing signals, and hence differentiate into PE as a result of position. (b) 'Salt and Pepper' model: cells sort according to their gene expression patterns. (c) New model of PE formation, emphasising the importance of both position and gene expression.

Table 1

Origin of surface cells

Blastocyst [*]	Duration of tracking	Nb of surface daughter cells[a]	% with a surface origin [b]	Nb of distinct lineages on the surface at the end [c]	% restricted to the surface [d]
2604_b2	29h45	16	44%	8	50%
2604_b3	29h45	19	79%	6	67%
2604_b4	27h30	14	64%	8	63%
1608_b5	17h30	14	86%	7	57%
2301_b3	24h45	11	55%	7	29%
2301_b4	24h45	26	42%	10	40%
2301_b5	24h45	21	52%	7	43%
pooled data		*121*	*59%*	*53*	*49%*

[*] see Fig. S2D for the number of cells per embryo

[a] number of cells with a surface fate, at the time of apoptosis or at the end of imaging (for example cells 1b and 8a in Fig. 3F).

[b] percentage of these cells arising from a mother cell lying at the surface initially.

[c] number of lineages with surface daughter cells which did not undergo apoptosis.

[d] percentage of these lineages which did not also contribute to the deeper ICM.

Table 2

Summary of the origin and fate of all tracked ICM cell lineages.

| | | fate | | |
		surface only	**mixed**	**deeper only**
origin	surface	19	11	12
	deeper	7	16	12
		34%	35%	31%